X-ray phase vortices: theory and experiment

Andrew G. Peele, Keith A. Nugent, and Adrian P. Mancuso

School of Physics, University of Melbourne, Parkville, Victoria 3010, Australia

David Paterson and Ian McNulty

Advanced Photon Source, Argonne National Laboratory, 9700 South Cass Avenue, Argonne, Ilinois 60439

Jason P. Hayes

Industrial Research Institute Swinburne, Swinburne University of Technology, Hawthorn 3122, Australia

Received November 23, 2003; revised manuscript received February 24, 2004; accepted March 29, 2004

We review the current work on x-ray phase vortices. We explain the role of an x-ray vortex in phase recovery and speculate on its possible applications in other fields of x-ray optical research. We present our theoretical understanding of the structure of phase vortices and test these predictions against experiment. We present experimental observations of phase vortices with charge greater than 3 and observe that their propagation appears to be consistent with our theoretical models. © 2004 Optical Society of America

OCIS codes: 340.0340, 340.6720, 350.7420.

1. INTRODUCTION

The field of singular optics is in a state of rapid development and is concerned with the properties and applications of an optical field that contains a phase singularity. Although undergraduate texts do not discuss such structures, and they can therefore seem unfamiliar, it is now well established that singular phase structures are ubiquitous, and they have been studied extensively in the visible optics wavelength regime. Only recently has it been demonstrated that singular phase structures can be observed at x-ray wavelengths.[1]

In a singular optical beam, a point discontinuity in the plane transverse to the axis of propagation occurs when the complex amplitude is zero; the phase at that point is therefore undefined. A surface of constant phase about the singularity can describe a helix that contains m turns for each wavelength traveled along the propagation axis, where m is an integer and is termed the topological charge of the optical singularity or vortex. These structures are noteworthy not just because of their interesting topology but also because they carry orbital angular momentum.[2–4]

There have been many investigations into the properties of optical vortices[5–7] and it is generally recognized that vortices are a common feature in the wave front of coherent light propagated through a real system.[8–10] The optical spanner effect of the transfer of orbital angular momentum from the vortex to a particle in the beam[11] is often cited as an application for vortex beams, although many other properties justify their study. For example, the so-called vortex-Bessel beams[12] form part of the set of nondiffracting beams. This, coupled with the fact that optical vortices also exhibit the ability to regenerate their initial phase distribution after propagation through an obstacle,[13] appears to offer promise in micromanipulation and in lithography. Optical vortices have been generated in a controlled fashion by a variety of methods, including laser cavity modes,[14] cylindrical lens mode conversion of laser modes,[15] computer-generated holograms—including spiral zone plates[16] and forked diffraction gratings[17]—and phase plates.[18–20]

It has been demonstrated that it is possible to generate a vortex by use of a spiral phase plate in the partially coherent x-ray light of a third-generation synchrotron.[1] However, there have been suggestions that high charge vortex states will be inherently unstable on propagation[5] because of interaction with interfering wave fields such as a component of coherent scatter.[21] In visible wavelength singular optics, where sources of coherent light are better controlled than for x rays, charge states greater than 100 have been demonstrated.[22] In the synchrotron context, where transmission elements, mirrors, and diffraction elements such as monochromators are an integral part of any experiment, there will always be a source of coherent scatter and so it is not clear whether propagated high charge vortices will be observed.

Here we collect and review the work to date in x-ray vortices, discuss it in more detail, and extend the experimental results to observations of high charge states. In Section 2 we speculate on some ambitious applications of x-ray vortices. Section 3 addresses our primary interest in x-ray vortices that relates to their role in wave-field recovery techniques. In Section 4 we review our theoretical understanding of the properties of vortices, and we discuss how they can be unambiguously created and verified. In Section 5 we present the experimental methods, and Section 6 describes the results. We draw our conclusions in Section 7 and summarize the paper in Section 8.

1084-7529/2004/081575-10$15.00

2. APPLICATIONS OF X-RAY VORTICES

Physically, vortices are characterized by a true zero in the intensity distribution that is stable under propagation. This feature might be exploited in a number of applications. Our principal rationale for exploring phase vortices is described in the Section 3 where we discuss the role of vortices in phase and wave-field retrieval. However, before doing so we briefly speculate on some additional areas of practical application for x-ray vortices.

- Lithography: The stable topological features of vortex beams might encourage their application to x-ray wave fields and an exploration of their uses in lithography and other forms of x-ray imaging. In particular, we note that collimation of x-ray fields is a possibility by the introduction of nondiffracting structures, such as Bessel beams that contain a phase singularity.[12] We note that the vortex itself might be regarded, in the near field, as a self-assembled optical structure with a characteristic scale equal to the wavelength of the radiation.
- X-ray astronomy: There has been a proposal to use the intensity zero in a vortex core as a window through which to observe a faint feature very close to a very bright feature.[23] Given the success of high-resolution x-ray imaging observatories such as NASA's Chandra X-Ray Observatory, this approach might be a feasible method by which to examine a weak x-ray background signal hidden in the glare of a bright coherent source. More recently, there has been a consideration of various astrophysical processes that might produce light with orbital angular momentum (i.e., a vortex beam).[24] Several of these situations, including imprinting vortex phase by passage through density inhomogeneities, transfer of orbital angular momentum by Kerr black holes, and artificial vortex beams generated by extraterrestrials, could easily arise at x-ray wavelengths. Detection of single photons with orbital angular momentum, which is possible at visible wavelengths,[25,26] would be difficult for x rays. But if fluxes should be significant, then the techniques described in Sections 4 and 5 could be useful.
- Microscopy: In principle the dark core of a vortex has a physical scale comparable with that of the wavelength of the light, and, because the vortex core might be regarded as a self-assembled optical structure, is largely independent of the optics creating the light wave. It might therefore be possible to create a vortex at the center of a focal spot and use the structure to enhance the resolution of, for example, a scanning x-ray microscope.
- Micromachines: The transfer of orbital angular momentum from the light beam to small particles in the so-called optical spanner application is well known.[11] The effect requires photons to be absorbed by the object to be rotated. At x-ray wavelengths an additional degree of freedom might be exploited because absorption rises dramatically at edge energies. Thus a component made of copper might be made to rotate at 8 keV ($\lambda = 0.15$ nm) whereas a tungsten component, also in the rotation orbit, would remain stationary.

All the above proposals have yet to be experimentally demonstrated, however they suggest that the additional optical feature accorded by phase vortices might find application in a number of yet to be explored areas.

3. X-RAY VORTICES AND PHASE RECOVERY

A phase vortex is characterized by two important features: a zero in the intensity distribution at the point at which the phase is not defined and the structural stability of the vortex. Since angular momentum must be conserved, the phase structure cannot disassemble without interacting with some other structure. The structural stability leads to the importance of phase vortices in the study of phase recovery. Although interferometry can be performed by use of x rays, it is inconvenient in many circumstances and so alternative approaches have been developed. These noninterferometric techniques are becoming an increasingly important tool in the context of x rays because of their flexibility as well as their ability to access the full complex refractive index of a material[27] and to image samples at high resolution.[28]

Phase retrieval methods can be categorized into methods that apply in the Fraunhofer region and methods that apply in the Fresnel region. In the Fraunhofer region techniques include conventional crystallographic methods and the iterative methods (now known as oversampling methods) based on the ideas of Gerchberg and Saxton,[29] Bates,[30] Fienup,[31] and Sayre and Chapman,[32] and they have been experimentally demonstrated by Miao *et al.*[28] and subsequent researchers.[33] The Bates[30] discussion of these approaches identified four trivial ambiguities that such methods cannot resolve, one of which is the inability to distinguish two fields related through phase conjugation. As will be seen, this ambiguity implies that certain vortex fields cannot be distinguished by use of oversampling approaches. It is worth noting that vortex phase structures are often created in phase solutions obtained by use of iterative phase recovery methods and are usually artificially eliminated on the grounds that they are nonphysical.[34] While it is true that the elimination of these phase structures is often correct, it is worth noting that the elimination must be based on physical arguments that relate to the form of the expected field and not on *a priori* assumptions about the impossibility of vortex phases being created by nature.

More recently, Nugent *et al.*[35] considered the oversampling methods from a symmetry perspective and have shown that fields can be recovered uniquely if one is able to utilize modern x-ray optics technology to shape the phase of the illuminating field. This approach breaks the symmetry of the diffracted field and so allows the ambiguities identified by Bates[30] (and others, such as homometric structures[36]) to be resolved. This approach has yet to be experimentally demonstrated, but some results obtained by Robinson *et al.*[37] are suggestive.

Noninterferometric phase recovery methods have also been developed and demonstrated in the Fresnel region. These include both direct and iterative methods. The iterative oversampling methods in the Fraunhofer region are based on the result that the far-field intensity diffraction pattern of a finite object defines the object structure *almost* uniquely.[30] Fresnel region methods use the result that the rate of change of the intensity of a field uniquely defines that field provided that the intensity is always positive. The concomitant is that a zero in intensity al-

lows for the presence of a phase discontinuity such as a vortex. In this way, the role of phase discontinuities in phase recovery becomes apparent.

An important direct method is based on the transport of intensity equation. We now consider this approach in the context of the Poynting vector **S**. The Poynting vector describes a vector field that, in general, can be described by a scalar and vector potential:

$$\mathbf{S}(\mathbf{r}) = I(\mathbf{r})[\nabla\Phi_S(\mathbf{r}) + \nabla \times \mathbf{\Phi}_\nu(\mathbf{r})], \tag{1}$$

This way of writing the Poynting vector has been discussed elsewhere.[38] If we introduce a paraxial approximation, the rate of change of intensity along the optical axis has the form

$$k\frac{\partial I(\mathbf{r})}{\partial z} = \nabla_\perp \cdot \mathbf{S}(\mathbf{r}_\perp), \tag{2}$$

where k is the wave number, and the $\perp$ subscript indicates that the vector or operator is two dimensional and acts only in the plane perpendicular to the optical axis. All subsequent discussion will assume paraxiality, and we drop this subscript for the remainder of this paper. Substituting Eq. (1) into Eq. (2) gives[38]

$$k\frac{\partial I(\mathbf{r})}{\partial z} = \nabla \cdot [I(\mathbf{r})\nabla\Phi_S(\mathbf{r})] + \nabla I(\mathbf{r}) \cdot \nabla \times \mathbf{\Phi}_\nu(\mathbf{r}), \tag{3}$$

This expression immediately reveals the possibility of hidden phases with the property that

$$\nabla I(\mathbf{r}) \cdot \nabla \times \mathbf{\Phi}_\nu(\mathbf{r}) = 0. \tag{4}$$

Phase vortices are easily shown to be an example of a phase structure that obeys this condition. More generally, the requirement of vorticity indicates that these phase terms carry angular momentum. The presence of an intensity zero, without which the phase is uniquely defined,[39] implies the presence of a phase vortex. Moreover, the form of Eq. (3) implies that the fundamental problem is one of symmetry, which links this observation with the structured phase far-field method proposed by Nugent *et al.*[35]

In general, phase recovery implies that the field has a high degree of coherence, although propagation-based phase methods have been generalized to the partially coherent case.[38] More general wave-field recovery methods have been proposed. Based on projections,[40,41] these allow the recovery of correlations (or, from a quantum mechanics perspective, the density matrix) from intensity measurements. These methods have been demonstrated in one dimension in the quantum optics application,[42] and recently in the x-ray optics application.[43] In the two-dimensional context, the correlation function is four dimensional, and it has been shown that the presence of vortex fields does not allow the unique recovery of correlations from three-dimensional intensity measurements.[44] It has also been shown that the introduction of cylindrical lenses allows the unique recovery of correlation information.[41] The symmetry breaking requirement implied by use of cylindrical lenses suggests that the presence of vortices is not only an example[44] of indeterminism but is necessary.

In summary, it is our contention that x-ray vortex structures play a central role in a full appreciation of the properties of x-ray wave fields and so these structures must be understood for the full development of the field of coherent x-ray optics.

4. THEORETICAL TREATMENT

In this section we present a basic formalism applicable for phase vortices placed in a synchrotron x-ray beam. This discussion is a summary of results presented elsewhere.[45] We model the synchrotron light field as a Gaussian beam with constant phase at the source and amplitude given by

$$u(r,\ \theta,\ 0) = \sqrt{\frac{2}{\pi}}\,\omega_0 \exp\left(-\frac{r^2}{{\omega_0}^2}\right), \tag{5}$$

where r and θ are polar coordinates and ω_0 is the $1/e$ half-waist at $z = 0$. As discussed in Section 3, vortices are potentially present in all diffraction regimes. In the synchrotron context of our experiments, the maximum dimension in the phase plate or detector was of the order of 1 mm and the wavelength of the radiation was of the order of 0.1 nm. The Fresnel condition is therefore satisfied for propagation distances greater than approximately 1 cm, which is always the case in our experiments in which propagation distances are of the order of meters. Here we consider the Fresnel diffraction regime as appropriate for a range of x-ray experiments. This field can be propagated to a plane z_1 at which point a phase plate with transmission function

$$T(r,\ \theta) = \exp(im\theta) \tag{6}$$

is introduced.

We can then calculate the Fresnel propagation of this vortex beam by evaluating the Fresnel integral at some detector plane $Z = Z' - z_1$, where Z' is the distance of the detector plane from the synchrotron source. After some calculation and simplification this becomes

$$\begin{aligned} u(R,\ \Theta,\ Z) = {} & A(Z)\exp[-A'(Z)R^2] \\ & \times \exp[-i(m\Theta - \Phi'(Z) - \Phi''(Z)R^2)] \\ & \times R\left[I_{1/2(m-1)}\left(\frac{\gamma^2}{8\beta}\right) - I_{1/2(m+1)}\left(\frac{\gamma^2}{8\beta}\right)\right], \end{aligned} \tag{7}$$

where R and Θ are polar coordinates in the detector plane; I_n is a modified Bessel function of the first kind of order n;

$$\begin{aligned} A(Z) \equiv {} & \sqrt{\pi}\frac{2\pi}{\lambda Z}\frac{1}{\lambda z_1}\sqrt{\frac{2}{\pi}}\frac{1}{\omega(z_1)}\frac{k}{8Z} \\ & \times \left\{\frac{1}{\omega(z_1)^4} + \left(\frac{\pi}{\lambda}\right)^2\left[\frac{1}{\Re(z_1)} - \frac{1}{Z}\right]^2\right\}^{-3/4}; \end{aligned} \tag{8a}$$

$$A'(Z) \equiv \left(\frac{k}{Z}\right)^2 \frac{1}{8} \frac{1}{\omega(z_1)^2} \times \left\{ \frac{1}{\omega(z_1)^4} + \left(\frac{\pi}{\lambda}\right)^2 \left[\frac{1}{\Re(z_1)} - \frac{1}{Z}\right]^2 \right\}^{-1}; \tag{8b}$$

$$\Phi'(Z) \equiv \pi - m\frac{\pi}{2} + kz_1 - \Psi(z_1) - \frac{3}{2}\arctan\left\{ \left(\frac{\pi}{\lambda}\right) \omega(z_1)^2 \left[\frac{1}{\Re(z_1)} - \frac{1}{Z}\right] \right\}; \tag{8c}$$

$$\Phi''(Z) \equiv \frac{k}{2Z} + \left(\frac{k}{Z}\right)^2 \frac{1}{8} \frac{\pi}{\lambda} \left[\frac{1}{\Re(z_1)} - \frac{1}{Z}\right] \times \left\{ \frac{1}{\omega(z_1)^4} + \left(\frac{\pi}{\lambda}\right)^2 \left[\frac{1}{\Re(z_1)} - \frac{1}{Z}\right]^2 \right\}^{-1}; \tag{8d}$$

$$\beta \equiv \frac{1}{\omega(z_1)^2} + i\frac{\pi}{\lambda}\left[\frac{1}{\Re(z_1)} - \frac{1}{Z}\right]; \qquad \gamma \equiv \frac{Rk}{2}; \tag{8e}$$

$$\omega(z) \equiv \omega_0\left[1 + \left(\frac{z}{z_R}\right)^2\right]^{1/2}; \qquad \omega(z) \equiv \omega_0\left[1 + \left(\frac{z}{z_R}\right)^2\right]^{1/2};$$

$$\Psi(z) \equiv \arctan\left(\frac{z}{z_R}\right); \qquad \Re(z) \equiv z\left[1 + \left(\frac{z_R}{z}\right)^2\right];$$

$$z_R \equiv \frac{\pi {\omega_0}^2}{\lambda}; \qquad k = \frac{2\pi}{\lambda}. \tag{8f}$$

The detected intensity is given by

$$I(R, \Theta, Z) = |u(R, \Theta, Z)|^2. \tag{9}$$

In our experimental results we used beam-defining slits and so we model the source as equivalent to being produced by a symmetric Gaussian with appropriate width. A plot of Eq. (9) is shown in Fig. 1 for the synchrotron parameters $z_1 = 41.4$ m, $\omega_0 = 200$ μm, $\lambda = 0.14$ nm, and with $Z = 5.8$ m. Note the intensity zero at the center of the vortex, and note also that the intensity variation is purely radial, whereas the vortex phase in Eq. (7) contains an azimuthal component. This indicates that the hidden phase condition of Eq. (4) is satisfied. Note also that a change in sign of the topological charge represents a phase conjugation process and so corresponds to one of the trivial phase ambiguities identified by Bates.[30]

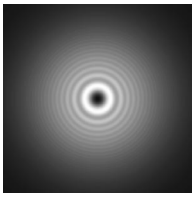

Fig. 1. Calculated intensity for an ideal theoretical vortex calculated by use of Eq. (9). The synchrotron parameters used were $z_1 = 41.4$ m, $\omega_0 = 200$ μm, $\lambda = 0.14$ nm, and $Z = 5.8$ m.

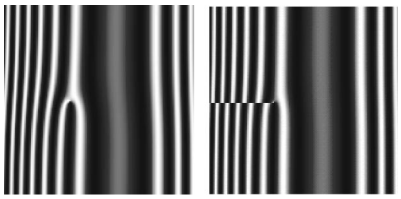

Fig. 2. Modulation to the intensity distribution of Eq. (10) produced by the cosine of θ_{interf} given by (a) Eq. (11): $\lambda = 0.14$ nm, $Z = 5.8$ m, $x_{\text{offs}} = 42.5$ μm, and $z_{\text{offs}} = 3$ mm and (b) the modified form of Eq. (11) discussed in Subsection 4.B: $\lambda = 0.14$ nm, $Z = 5.8$ m, $x_{\text{offs}} = 42.5$ μm, $z_{\text{offs}} = 3$ mm, and $\nu = 0.5$.

A. Interferograms Produced by Division of the Wave Front

In practice the existence of a vortex is not demonstrated merely by producing the type of intensity distribution shown in Fig. 1. Ideally some demonstration of the phase distribution should be made and interferometric methods are most explicit.

It is experimentally difficult to create an x-ray vortex wave front that can be analyzed by a division of amplitude interferometer such as a Bonse–Hart interferometer. We therefore consider the use of a division of wave-front technique based on the introduction of a wire so that the wave diffracted by the wire interferes with the vortex wave. In this subsection we summarize a model of this system.[45]

The detailed experimental system is discussed in Section 5. However, we note that the wire is placed close to the phase plate, and we analyze the experiment as if it were the interference of the vortex beam in Eq. (7) and a cylindrical wave diffracted by the wire. Strictly, the wave generated by the wire will not be a cylindrical wave because of the curvature in the beam and the vortex phase imparted by the phase plate. However, we find the approximation to be valid when we use a numerical simulation for the synchrotron parameters. Given this, the resulting intensity is

$$I = {A_v}^2 + A_{\text{cyl}}^2 + 2A_v A_{\text{cyl}} \cos\theta_{\text{interf}}, \tag{10}$$

where A_v is the amplitude of the vortex beam given by Eq. (7), A_{cyl} is the amplitude of the cylindrical wave, and there is a modulation to the intensity distribution given by the cosine of the interference term

$$\theta_{\text{interf}} = \left\{ -m\arctan\left(\frac{y}{x}\right) + kZ + k[(x - x_{\text{offs}})^2 + (Z - z_{\text{offs}})^2]^{1/2} + m\arctan\left(\frac{y}{x_{\text{offs}}}\right) \right\}, \tag{11}$$

where x_{offs} and z_{offs} are the offset coordinates of the wire with respect to the phase plate.

Figure 2(a) shows the modulation to the intensity distribution produced by the cosine of θ_{interf} given by Eq. (11). It can be seen that the phase discontinuity introduces a fork in the fringe pattern.

B. Vortex and an Edge Discontinuity: Noninteger Charge

In this work, the vortex is created by passing the x rays through a phase plate such that a phase ramp of height $2\pi m$ is imparted onto the wave. However thickness errors in the phase plate manufacture are inevitable. The result is a mixed vortex and edge dislocation as has been described in earlier papers.[5]

In general the charge of the spiral will be some noninteger ν. In this case, the derivation of Eq. (7) is modified by replacing m with ν and the Bessel function of the first kind of order m becomes a sum of an Anger and a Weber function of the first kind of order ν. Although not strictly correct,[45] we find that simply replacing m with ν in Eq. (11) is a good approximation for the conditions explored in the present paper.[45] The approach here becomes similar to that taken elsewhere in calculating the hologram and demonstrating the production of a vortex,[10] including noninteger charge vortices.[46] Figure 2(b) shows a plot of the cosine of the modified form of θ_{interf} given by Eq. (11) with $\nu = 0.5$.

In the synchrotron context it is relatively straightforward to continually vary the incident energy over a broad range. The charge of the phase plate will vary as a function of the refractive-index decrement times the energy. Away from absorption edges the refractive-index decrement is roughly inversely proportional to the square of the energy, so the charge will be roughly inversely proportional to the energy in this regime.

5. EXPERIMENTAL METHODS

An x-ray phase plate was manufactured with a Mask Projection Micromachining System (Exitech Series 8000)[47] utilizing a Lambda Physik LPX210i krypton fluoride excimer laser operating at 248 nm. A conventional chrome-on-quartz mask was used to define the irradiated area and has a lateral resolution of approximately 1 μm. It was not possible to create a smooth phase ramp in the polyimide substrate. Accordingly, excimer laser ablation was used, with a series of indexed masks overlaid on the substrate to produce a 1-mm-diameter spiral staircase structure approximating a spiral ramp. The depth of individual steps was varied by adjusting the laser fluence and/or the number of pulses used. A sample result obtained with 15 indexed masks is shown in Fig. 3.

In the structures used to create a charge 1 vortex the total depth of the spiral was measured with a confocal microscope to be 34.2 ± 0.5 μm, corresponding to a phase ramp of $(1.90 \pm 0.03)\pi$ for 9-keV ($\lambda = 0.14$-nm) x rays. Note that because the real part of the refractive index can be written $n_R = 1 - \delta$, where δ is a small positive number in the x-ray regime, the ramp will induce a phase advance rather than the delay familiar from visible optics. For polyimide at 9 keV ($\lambda = 0.14$ nm), as used in the present work, $\delta \cong 3.83 \times 10^{-6}$. Inaccuracies in the overlay procedure coupled with the inherent resolution of the system meant that an approximately 30-μm-diameter central area of the spiral was poorly defined, as can be seen in Fig. 3. At the x-ray energy of 9 keV ($\lambda = 0.14$ nm) used here, transmission through the thickest part of the polyimide spiral is 99%, thus making our spiral staircase essentially a phase-only structure at this energy.

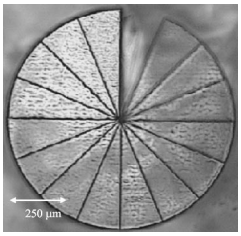

Fig. 3. Microscope image of one of the 16-step phase plates used in the experimental work. The surface roughness of each step can be seen to increase in a clockwise direction around the phase plate, indicating the increase in depth of each step.

We performed imaging experiments at the Sector 2 Insertion Device branch beamline (2-ID-D) at the Advanced Photon Source, Argonne National Laboratory. The undulator source provides a coherent flux (10^{10}–10^{12} photons/s/0.1% BW) of x rays in the 2–32-keV range ($\lambda = 0.62$–0.04 nm). The beam is defined by a series of slits and mirrors and by a double-crystal monochromator ($E/\Delta E = 7000$). Using a procedure reported elsewhere[48] the horizontal coherence length, for the slit settings used on the 2-ID-D, was measured to be well in excess of 30 μm.[48] The vertical coherence is governed by the effective source size and, for the settings used, was of a similar size to the horizontal coherence length. As this exceeds the size of the poorly defined region in the center of the spiral, we expect this will have a minor effect on the generation of the x-ray vortex. The spiral phase plate was placed in air a short distance from the exit window of the beamline. The vortex beam was observed after a propagation distance of 5.8 m through an evacuated flight path by use of an imaging detector comprising a doped cadmium tungstate crystal scintillator magnified through an objective lens onto a CCD camera to produce an effective pixel size of 0.61 μm $\times$ 0.61 μm. The CCD camera chip contained 1317 $\times$ 1035 pixels.

6. EXPERIMENTAL RESULTS

A. Charge 1 Vortex

The vortex is expected to show a dark core surrounded by a brighter ring (see Ref. 1). Figure 4 shows the observed distribution. A bright ring is evident, though not obvious. However the dark core is clearly observed as indicated by the data in the insert in Fig. 4, which shows the average of a vertical and horizontal intensity trace through the center of the vortex core. The diffraction observed along the edge of the largest physical step in the structure is not due to a phase mismatch but to the machined structure, which has a 7° slope in the wall of each step. In the largest step this forms a long enough ramp to produce the observed fringes. In our experimental setup it is difficult to confirm a true zero in intensity. The scintillator crystal and windows, mirrors, and gas in the nonevacuated parts of the flight path all contribute to scatter that fills in any intensity zeros in the field. Nonetheless, the dip at the vortex shown in Fig. 4 is consistent with an intensity zero at the vortex core.

This experiment is simulated with the known properties of the system. It was observed that the roughness on the phase plate surface increased with the depth of the ablation. The effect of the roughness was simulated by including a Gaussian distribution of random heights, the statistical properties of which were based on measurements taken with optical confocal microscopy and direct x-ray radiography. A simulation was performed with a 2π maximum phase step in the phase plate to confirm that the intensity distribution revealed in these data did indeed conform to the expected structure. The result of the simulation as compared with the experimental result is shown in Fig. 5.

An intensity distribution of the form shown in Fig. 4 can exist without the presence of a vortex. The signature of a vortex is unambiguously revealed in the phase information. In an interference pattern this corresponds to the appearance of a fork in the fringe structure. We therefore chose to use a division of wave-front interferometer to determine the phase structure in the wave front. In this case, because of the energetic photons, we simply split the wave field by introducing a 7.5-μm-diameter tungsten wire 3 mm behind the phase plate. To isolate the presence of the vortex, images were recorded both with and without the phase plate. The result with the phase plate is shown in Fig. 6(a). The fork in the interference fringes, characteristic of a vortex phase discontinuity, is clearly apparent. The result without the phase plate shows simply the expected Fresnel diffraction fringes produced by a wire and is shown in Fig. 6(c). We also performed a similar set of experiments in which a transparent edge, also acting as a division of wave-front interferometer, was scanned across the vortex. As the edge moved further away from the vortex core, the forked fringe shifted from the first to the second and then the third fringe while remaining at the same position with respect to the phase plate. Examples of these results are shown in Fig. 7. These observations further confirm the presence of a propagating vortex structure.

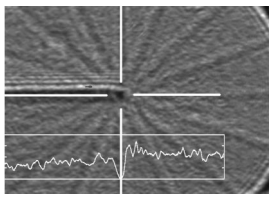

Fig. 4. Diffracted intensity produced by a 16-step phase plate for $Z = 5.8$ m and $\lambda = 0.14$ nm measured with a crystal scintillator and a CCD camera. The circular edge of the ~1-mm-diameter phase plate can be seen. The inset shows the intensity as measured through the core and along the vertical and horizontal lines shown on the image.

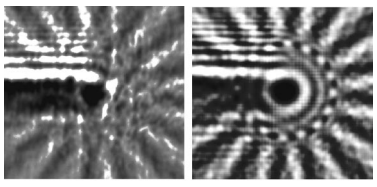

Fig. 5. (a) Magnified portion of another experimental image as reported for Fig. 4. (b) Simulation of the same experiment done with the known experimental parameters as described in the text.

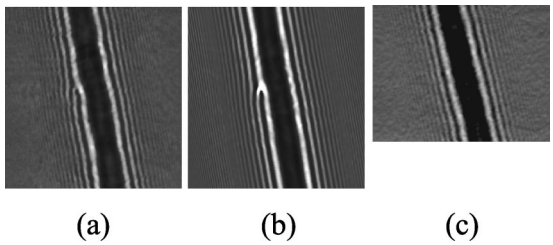

Fig. 6. (a) Experimental vortex interferogram produced by interfering the wave field produced by a 7.5-μm tungsten wire 3 mm downstream of the phase plate with the vortex wave field produced by the phase plate. The other experimental parameters are as for Fig. 4. (b) Simulation of the division of the wave-front interferogram experimental result shown in (a) done with the known experimental parameters and assuming a maximum phase shift of 1.8π. The result shows excellent agreement. (c) Same as for (a) but with the phase plate removed. The expected Fresnel fringes for the wire are seen with no splitting.

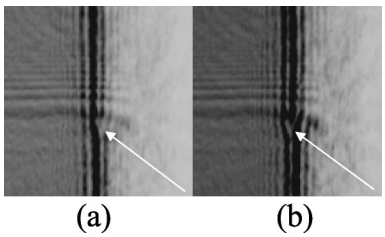

Fig. 7. Demonstration of the association of the position of the interferogram fork with the central position of the phase plate produced by movement of an edge relative to the phase plate. As indicated by the arrows, the fork moves from the second diffraction fringe of the edge in (a) to the third fringe and in (b) as the edge is moved with respect to the phase plate.

The interferogram patterns can also be simulated by incorporating the effect of the wire and the effect of using different thickness phase plates. As phase thickness is increased from zero to 2π, the fringe pattern evolves from the straight-line diffraction pattern produced by a wire alone to the forked pattern shown in Fig. 6(b). The exact evolution depends on the orientation of the physical discontinuity in the phase plate; if the phase plate produces a phase shift that is not an integer multiple of 2π, then the wave front acquires an additional edge dislocation in the phase, which has an effect on the propagation. It is possible to minimize the difference between the simulated and the experimental images as a function of phase shift and orientation of the phase plate to obtain an estimate of the maximum x-ray phase shift. Because of uncertainties in our experimental data and in the simulation itself, we do not consider our estimate of the maximum phase shift to be accurate to better than $\pm 10\%$. The simulation gives an estimate of the maximum phase shift as $(1.8 \pm 0.2)\pi$, which is in agreement with the value based on measurement of the phase plate thickness. The interferogram corresponding to the best estimate is shown in Fig. 6(b) and is in excellent agreement with the data in Fig. 6(a).

B. Negative Charge Vortices

An additional confirmation of the phase structure is obtained by observing the interferogram with the phase

plate reversed, which corresponds to a sign change in the charge and results in a fork with the opposite orientation.[21] Figure 8 shows a pair of interferograms into which the phase plate is inserted first one way and then the other. The expected change in the orientation of the fork is apparent.

C. Higher Charge Vortices

To examine the properties of a higher charge vortex, we used 32-step spiral staircase approximations to a phase ramp machined into a polyimide substrate. To unambiguously identify the presence and charge of a vortex, as before, we generated an interference pattern using a division of wave-front interferometer in the form of a 7.5-μm tungsten wire placed a short distance behind the phase plate. The expected interference pattern displays a fork with $m + 1$ branches, where m is the charge of the vortex.[46]

An image was taken with the wire and phase plate in place and another with just the phase plate. The latter image was used to divide the former and produce a clean interferogram from which structure due to the incident beam and the phase plate steps has been removed and the interference fringes can be clearly seen. Figure 9(a) shows an observation of a high charge vortex at 6 keV ($\lambda = 0.21$ nm), and Fig. 10(a) shows a sequence of images at different energies between 7 and 12 keV ($\lambda = 0.18$–0.1 nm). The phase plate used in Figs. 9(a) and 10(a) had an approximately 80-μm maximum step height corresponding to a charge range of approximately 3.3–1.7 for the energies used.

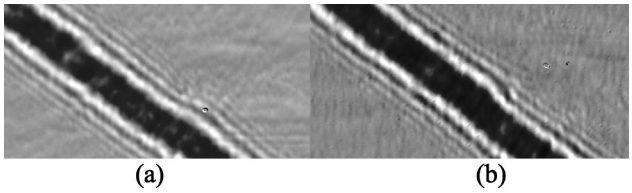

Fig. 8. Demonstration of negative charge: reversal of the fork direction by reversal of the phase plate.

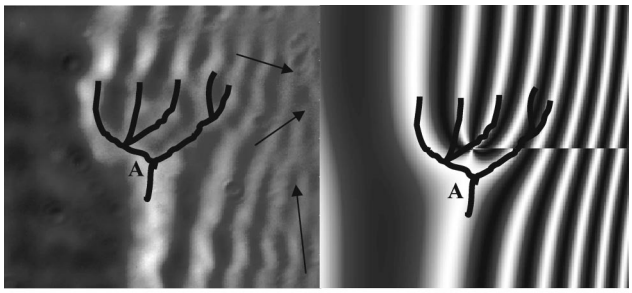

Fig. 9. (a) Experimental interferogram for a 32-step polyimide phase plate with a maximum step depth of ~80 μm measured at 6 keV ($\lambda = 0.21$ nm); the other experimental parameters are as described previously. The overlaid sketch shows the fringe positions with branching points with the label A indicating the first branch point. The arrows indicate the locations of additional single-charge vortices of the opposite sign to the main vortex. (b) Calculated interferogram for the phase plate at 6 keV ($\lambda = 0.21$ nm) by use of the modified form of Eq. (11) discussed in Subsection 4.B. The sketch from (a) is overlaid showing the fringe positions with branching points for the experimental data.

7. HIGH AND NONINTEGER CHARGE PROPAGATION

It has been suggested that, when a vortex is not centered in its host beam, it is then susceptible to splitting by the addition of another coherent wave, even of small amplitude.[21] Elsewhere[4] it has been argued that noninteger charge states will also be unstable. In this section we discuss whether this might explain the detailed structure seen in Fig. 9(a).

The theoretical discussion of the splitting of a vortex of charge m into m single-charge vortices predicts that the daughter vortices will each be displaced by a distance r_m from the center of the host beam given by[21]

$$r_m = \omega_0 \left(\frac{A}{A_m} \right)^{(1/|m|)} \frac{[z^2 + [k\omega_0^2/2]^2]^{1/2}}{(k\omega_0^2/2)}, \qquad (12)$$

where ω_0 is the host beam waist parameter; k is the wave number, z is the propagation distance, and A and A_m are

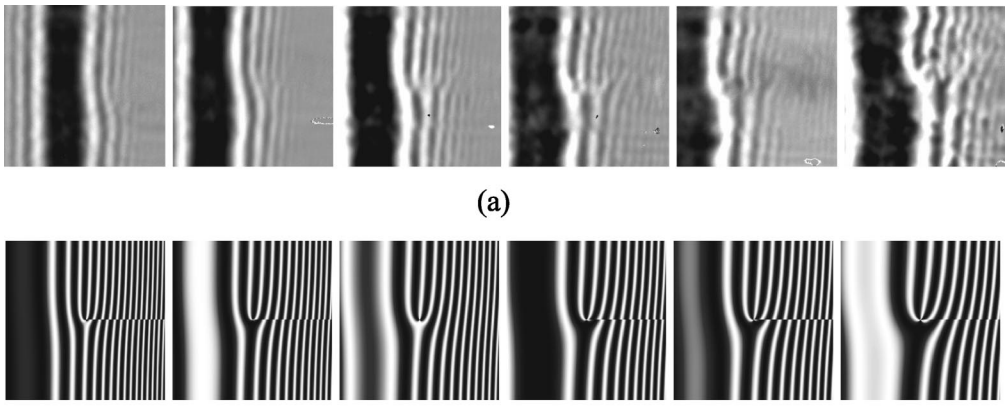

Fig. 10. (a) Experimental interferograms as for Fig. 9(a) for energies of 12–7 keV ($\lambda = 0.1$–0.18 nm) from left to right, decreasing in 1-keV steps. (b) Calculated interferograms as for Fig. 9(b) at the same energies as in (a). Note that the size and contrast in the region about the wire position will differ from the experimental data as the calculated images assume an infinitely narrow wire. However, the fringes to the side of the wire position are in good agreement with the data.

the amplitudes of the additive and host fields, respectively. In Fig. 9(a) a sketch overlay shows the fringe positions. There appear to be three separate forks in the fringes that represent two charge one vortices and a charge 2 vortex. A circle joining the three fork positions has radius of approximately 16 μm. For the experimental parameters for the result shown in Fig. 9(a), Eq. (12) is in agreement with this only when the amplitude ratio is approximately 1%. At 6 keV ($\lambda = 0.21$ nm) the total coherent scattering fraction for polyimide is only a few percent and is angle dependent and forward peaked.[49] However, the solid angle subtended by the detector for our experiment is only approximately 2.8×10^{-8} sr. Even allowing for forward peaking of the scattering distribution, the solid angle subtended by the detector here will reduce the amplitude ratio several orders of magnitude below the 1% required for Eq. (12) to agree with the data. A reduction to 10^{-4}% (corresponding to a much stronger forward peaking than might be expected experimentally[50]) results in a splitting radius of only 1 μm. Another explanation of the observed structure is therefore needed. It should also be noted that the earlier experimental observations of high charge splitting[21] are in the Fraunhofer region and that no splitting was seen in the Fresnel region. We are able to conclude, however, that the observed core splitting can be explained without invoking the effect of coherent interactions within the beam.

At most energies the phase step across the phase plate was not an integer multiple of 2π. Accordingly, it may be that the fork positions are simply the actual fork positions for the noninteger charge of the phase plate. As can be seen from Figs. 9(a) and 10(a), during the evolution of increasing charge the fringes appear in different places as they merge into a single multiple fork—corresponding to an energy where the charge is integer. The phase plate in the noninteger charge cases would represent a line discontinuity that terminates at the middle. In Section 4 we showed that the resulting interferogram fringes can be approximately calculated by evaluating the cosine of the interference phase angle between a plane wave with an embedded vortex phase and a cylindrical wave with an offset vortex phase given by a modified form of Eq. (11). Figure 10(b) shows the same series as for Fig. 10(a) calculated by using the modified form of Eq. (11) with nominal charges. Figure 9(b) shows the calculated image corresponding to Fig. 9(a). It can be seen that the general evolution to more forks is followed well.

The line discontinuity is not seen in the data because of the processing described above. However, because the experimental phase plate had a slope on all edges, the line discontinuity is blurred and fringes appear kinked but continuous across it. The differences between fork patterns in the calculated and the experimental data appear to be attributable to the distortion that is due to the difference between an ideal and the nonideal line discontinuity. Accordingly, the general pattern of fringes can be sketched for the data and overlaid onto the calculated pattern reasonably well, as is shown in Figs. 9(a) and 9(b), where the main discrepancy is a shifting of the fork junction across the line discontinuity. A similar exercise can be conducted for the images in Figs. 10(a) and 10(b). In Fig. 9 it can also be seen that the initial apparent fork split, labeled A in Figs. 9(a) and 9(b), is a feature of the way the forks appear rather than an actual split. From Figs. 10(a) and 10(b) it can also be seen that the apparent vortex splitting is consistent with the expected fork positions for a noninteger charge.

Close examination of Fig. 9(a) indicates the presence of additional fringe splitting (shown by arrows) to the right of the implanted vortex. These could have been implanted in the beam by the structure of the phase plate. Alternatively, the appearance of new vortices is an expected feature of propagation of vortex beams under certain conditions[51] and underlines the contention of this paper that x-ray vortices are ubiquitous in x-ray optics.

8. CONCLUSIONS

Singular optics is an important developing area in visible optics, and singular phase structures have very recently been reported in the x-ray region, as reviewed in this paper. The interest in such structures has a different motivation in x-ray optics where, as we understand them now, their importance arises from their role in complicating the process of phase recovery by use of noninterferometric methods both in the Fresnel regime and in the Fraunhofer diffraction regime. We have emphasized that phase vortices are real physical structures that cannot be automatically excluded from a phase solution obtained with iterative phase recovery methods.

The aim of this work was to demonstrate conclusively that x-ray phase vortices do exist, that they can be understood by use of methods developed for visible optics, and that higher charge vortices appear to be stable under propagation. We have therefore extended the analytical results to apply to the geometry appropriate to a synchrotron experiment and have experimentally tested the results at a third-generation synchrotron. We have also presented experimental results showing vortex beams with high and noninteger charges. The observations are consistent with the propagation of a noninteger charge vortex and do not require the introduction of coherent interactions to be understood.

It is possible that vortex beams such as these may find other applications, such as those outlined in Section 3. However, it is certainly true that an understanding of phase vortex structures is important for the full development and exploitation of coherent x-ray optics, and it is hoped that this paper provides a solid foundation from which these objects may be further studied and exploited.

ACKNOWLEDGMENTS

The authors acknowledge the support of Australian Research Council Fellowship funding. This research was supported by the Australian Synchrotron Research Program, which is funded by the Commonwealth of Australia under the Major National Research Facilities Program, and by the Australian Research Council. Use of the Advanced Photon Source was supported by the U.S. Department of Energy, Office of Science, Basic Energy Sciences, under contract W-31-109-ENG-38.

Address correspondence to A. G. Peele at peele @physics.unimelb.edu.au.

REFERENCES

1. A. G. Peele, P. J. McMahon, D. Paterson, C. Q. Tran, A. P. Mancuso, K. A. Nugent, J. P. Hayes, E. Harvey, B. Lai, and I. McNulty, "Observation of an x-ray vortex," Opt. Lett. **27**, 1752–1754 (2002).
2. L. Allen, M. W. Beijersbergen, R. J. C. Spreeuw, and J. P. Woerdman, "Orbital angular momentum of light and the transformation of Laguerre–Gaussian laser modes," Phys. Rev. A **45**, 8185–8189 (1992).
3. M. V. Vasnetsov, I. G. Marienko, and M. S. Soskin, "Self-restoration of an optical vortex," JETP Lett. **71**, 130–133 (2000).
4. M. Berry, "Paraxial beams of spinning light," in *International Conference on Singular Optics*, M. S. Soskin, ed., Proc. SPIE **3487**, 6–11 (1998).
5. J. F. Nye and M. V. Berry, "Dislocations in wave trains," Proc. R. Soc. London Ser. A **336**, 165–190 (1974).
6. M. S. Soskin and M. V. Vasnetsov, "Singular optics," in *Progress in Optics*, E. Wolf, ed. (Elsevier, New York, 2001), Vol. 42, pp. 220–276.
7. D. Rozas, C. T. Law, and G. A. Swartzlander, Jr., "Propagation dynamics of optical vortices," J. Opt. Soc. Am. B **14**, 3054–3065 (1997).
8. M. Harris, "Light-field fluctuations in space and time," Contemp. Phys. **36**, 215–233 (1995).
9. N. B. Baranova, B. Ya. Zel'dovich, A. V. Mamayev, N. F. Pilipetskii, and V. V. Shkukov, "Dislocations of the wavefront of a speckle-inhomogeneous field (theory and experiment)," Pis'ma Zh. Eksp. Teor. Fiz. **33**, 206–210 (1981) [JETP Lett. **33**, 195–199 (1981)].
10. Z. S. Sacks, D. Rozas, and G. A. Swartzlander, Jr., "Holographic formation of optical-vortex filaments," J. Opt. Soc. Am. B **15**, 2226–2234 (1998).
11. H. He, M. E. J. Friese, N. R. Heckenberg, and H. Rubinsztein-Dunlop, "Direct observation of transfer of angular momentum to absorptive particles from a laser beam with a phase singularity," Phys. Rev. Lett. **75**, 826–829 (1995).
12. S. Chávez-Cerda, G. S. McDonald, and G. H. C. New, "Nondiffracting beams: travelling, standing, rotating, and spiral waves," Opt. Commun. **123**, 225–233 (1996).
13. Z. Bouchal, "Resistance of nondiffracting vortex beam against amplitude and phase perturbations," Opt. Commun. **210**, 155–164 (2002).
14. M. Brambilla, F. Battipede, L. A. Lugiato, V. Penna, F. Prati, C. Tamm, and C. O. Weiss, "Transverse laser patterns. I. Phase singularity crystals," Phys. Rev. A **43**, 5090–5113 (1991).
15. M. W. Beijersbergen, L. Allen, H. E. L. O. van der Veen, and J. P. Woerdman, "Astigmatic laser mode converters and transfer of orbital angular momentum," Opt. Commun. **96**, 123–132 (1993).
16. N. R. Heckenberg, R. McDuff, C. P. Smith, and A. G. White, "Generation of optical phase singularities by computer-generated holograms," Opt. Lett. **17**, 221–223 (1992).
17. V. Yu. Bazhenov, M. S. Soskin, and M. V. Vasnetsov, "Screw dislocations in light wavefronts," J. Mod. Opt. **39**, 985–990 (1992).
18. M. W. Beijersbergen, R. P. C. Coerwinkel, M. Kristensen, and J. P. Woerdman, "Helical-wavefront laser beams produced with a spiral phaseplate," Opt. Commun. **112**, 321–327 (1994).
19. G. A. Turnbull, D. A. Robertson, G. M. Smith, L. Allen, and M. J. Padgett, "The generation of free-space Laguerre–Gaussian modes at millimetre-wave frequencies by use of a spiral phaseplate," Opt. Commun. **127**, 183–188 (1996).
20. G.-H. Kim, J.-H. Jeon, K.-H. Ko, H.-J. Moon, J.-H. Lee, and J.-S. Chang, "Optical vortices produced with a nonspiral phase plate," Appl. Opt. **36**, 8614–8621 (1997).
21. I. V. Basistiy, V. Yu. Bazhenov, M. S. Soskin, and M. V. Vasnetsov, "Optics of light beams with screw dislocations," Opt. Commun. **103**, 422–428 (1993).
22. J. E. Curtis, B. A. Koss, and D. G. Grier, "Dynamic holographic optical tweezers," Opt. Commun. **207**, 169–175 (2002).
23. G. A. Swartzlander, Jr., "Peering into darkness with a vortex spatial filter," Opt. Lett. **26**, 497–499 (2001).
24. M. Harwit, "Photon orbital angular momentum in astrophysics," Astrophys. J. **597**, 1266–1270 (2003).
25. J. Leach, M. J. Padgett, S. M. Barnett, S. Franke-Arnold, and J. Courtial, "Measuring the orbital angular momentum of a single photon," Phys. Rev. Lett. **88**, 257901 (2002).
26. H. Wei, X. Xue, J. Leach, M. J. Padgett, S. M. Barnett, S. Franke-Arnold, E. Yao, and J. Courtial, "Simplified measurement of the orbital angular momentum of single photons," Opt. Commun. **223**, 117–122 (2003).
27. P. J. McMahon, A. G. Peele, D. Paterson, K. A. Nugent, A. Snigirev, T. Weitkamp, and C. Rau, "X-ray tomographic imaging of the complex refractive index," Appl. Phys. Lett. **83**, 1480–1482 (2003).
28. J. W. Miao, P. Charalambous, J. Kirz, and D. Sayre, "Extending the methodology of x-ray crystallography to allow imaging of micrometre-sized non-crystalline specimens," Nature **400**, 342–344 (1999).
29. R. W. Gerchberg and W. O. Saxton, "A practical algorithm for the determination of phase from image and diffraction plane pictures," Optik (Stuttgart) **35**, 237–246 (1972).
30. R. H. T. Bates, "Fourier phase problems are uniquely solvable in more than one dimension. I: underlying theory," Optik (Stuttgart) **61**, 247–262 (1982).
31. J. R. Fienup, "Reconstruction of an object from the modulus of its Fourier transform," Opt. Lett. **3**, 27–29 (1978).
32. D. Sayre and H. N. Chapman, "X-ray microscopy," Acta Crystallogr., Sect. A **51**, 237–252 (1995).
33. J. M. Zuo, I. Vartanyants, M. Gao, R. Zhang, and L. A. Nagahara, "Atomic resolution imaging of a carbon nanotube from diffraction intensities," Science **300**, 1419–1421 (2003).
34. I. K. Robinson, Department of Physics, University of Illinois at Urbana–Champaign, Urbana, Ill. 61801 (personal communication, 2003).
35. K. A. Nugent, A. G. Peele, H. N. Chapman, and A. P. Mancuso, "Unique phase recovery for nonperiodic objects," Phys. Rev. Lett. **91**, 203902 (2003).
36. J. H. Seldin and J. R. Fienup, "Numerical investigation of the uniqueness of phase retrieval," J. Opt. Soc. Am. A **7**, 412–427 (1990).
37. I. K. Robinson, F. Pfeiffer, I. A. Vartanyants, Y. Sun, and Y. Xia, "Enhancement of coherent x-ray diffraction from nanocrystals by introduction of x-ray optics," Opt. Express **11**, 2329–2334 (2003), http://www.opticsexpress.org.
38. D. Paganin and K. A. Nugent, "Noninterferometric phase imaging with partially coherent light," Phys. Rev. Lett. **80**, 2586–2589 (1998).
39. T. E. Gureyev, A. Roberts, and K. A. Nugent, "Partially coherent fields, the transport-of-intensity equation, and phase uniqueness," J. Opt. Soc. Am. A **12**, 1942–1946 (1995).
40. K. A. Nugent, "Wave field determination using three-dimensional intensity information," Phys. Rev. Lett. **68**, 2261–2264 (1992).
41. M. G. Raymer, M. Beck, and D. F. McAlister, "Complex wave-field reconstruction using phase-space tomography," Phys. Rev. Lett. **72**, 1137–1140 (1994).
42. C. Kurtsiefer, T. Pfau, and J. Mlynek, "Measurement of the Wigner function of an ensemble of helium atoms," Nature **386**, 150–153 (1997).
43. C. Q. Tran, A. G. Peele, D. Paterson, A. Roberts, I. McNulty, and K. A. Nugent, "Correlations in a synchrotron beam measured using phase-space tomography," manuscript available from C. Q. Tran at tran@physics.unimelb.edu.au.
44. F. Gori, M. Santarsiero, and G. Guattari, "Coherence and the spatial distribution of intensity," J. Opt. Soc. Am. A **10**, 673–679 (1993).
45. A. G. Peele and K. A. Nugent, "X-ray vortex beams: a the-

oretical analysis," Opt. Express **11**, 2315–2322 (2003), http://www.opticsexpress.org.
46. I. V. Basistiy, M. S. Soskin, and M. V. Vasnetsov, "Optical wavefront dislocations and their properties," Opt. Commun. **119**, 604–612 (1995).
47. E. C. Harvey and P. T. Rumsby, "Fabrication techniques and their application to produce novel micromachined structures and devices using excimer laser projection," in *Micromachining and Microfabrication Process Technology III*, S.-C. Chang and S. W. Pang, eds., Proc. SPIE **3223**, 26–33 (1997).
48. J. J. A. Lin, D. Paterson, A. G. Peele, P. J. McMahon, C. T. Chantler, K. A. Nugent, B. Lai, N. Moldovan, Z. Cai, D. C. Mancini, and I. McNulty, "Measurement of the spatial coherence function of undulator radiation using a phase mask," Phys. Rev. Lett. **90**, 074801 (2003).
49. J. H. Hubbell, W. J. Veigele, E. A. Briggs, R. T. Brown, D. T. Cromer, and R. J. Howerton, "Atomic form factors, incoherent scattering functions, and photon scattering cross sections," J. Phys. Chem. Ref. Data **4**, 471–538 (1975).
50. A. Tartari, E. Casnati, C. Bonifazzi, and C. Baraldi, "Molecular differential cross sections for x-ray coherent scattering in fat and polymethyl methacrylate," Phys. Med. Biol. **42**, 2551–2560 (1997).
51. M. S. Soskin, V. N. Gorshkov, M. V. Vasnetsov, J. T. Malos, and N. R. Heckenberg, "Topological charge and angular momentum of light beams carrying optical vortices," Phys. Rev. A **56**, 4064–4075 (1997).